A comprehensive study on the atom flow in the cross-field discharge of a Hall thruster

2011 J. Phys. D: Appl. Phys. 44 105203

(http://iopscience.iop.org/0022-3727/44/10/105203)

IOP PUBLISHING JOURNAL OF PHYSICS D: APPLIED PHYSICS

J. Phys. D: Appl. Phys. **44** (2011) 105203 (8pp) doi:10.1088/0022-3727/44/10/105203

A comprehensive study on the atom flow in the cross-field discharge of a Hall thruster

S Mazouffre[1], G Bourgeois[1], L Garrigues[2] and E Pawelec[3]

[1] ICARE, CNRS, 1C avenue de la Recherche Scientifique, 45071 Orléans, France
[2] Toulouse University, UPS, INPT, LAPLACE, 118 route de Narbonne, F-31062 Toulouse cedex 9, France/CNRS, LAPLACE, F-31062 Toulouse, France
[3] Opole University, Oleska 48, Opole, Poland

E-mail: stephane.mazouffre@cnrs-orleans.fr

Received 21 September 2010, in final form 5 January 2011
Published 21 February 2011
Online at stacks.iop.org/JPhysD/44/105203

Abstract
The flow properties of Xe atoms were investigated in the 1 kW class PPS100-ML Hall effect thruster by means of Doppler-shifted laser-induced fluorescence spectroscopy in the near infrared. Fluorescence spectra of the 6s $[1/2]^o_2$ resonant level and the 6s $[3/2]^o_2$ metastable level have been acquired inside and outside the thruster channel under several operating conditions. Analytical treatment and modelling of the measured lineshapes indicate the atom axial velocity increases inside the channel to a value well above the sound speed before decreasing quickly in the near-field plume. Numerical simulations performed with a fluid/kinetic hybrid approach allow us to explain the shape of the velocity profile. Atomic flow acceleration originates in the combination of three processes, namely the selective ionization of slow atoms, the flow expansion and the creation of fast neutrals on BN-SiO_2 walls owing to recombination of ions. Deceleration results from the invasion of the atomic jet by slow and relatively cold atoms from the residual background gas and from the cathode. In addition, it is shown that charge-exchange collisions have a non-negligible impact on the atom velocity in spite of the low background pressure in test chambers.

(Some figures in this article are in colour only in the electronic version)

1. Background and goals

In a conventional chemical rocket engine, thrust originates in the expansion of a heated propellant through a solid nozzle. In an electric rocket engine, thrust results from the electrostatic acceleration of an ionized propellant. Therefore, electric thrusters achieve very high fuel exhaust speed which allows us to drastically reduce the loaded propellant mass, as shown by the Tsiolkovsky rocket equation [1]. Electric propulsion devices are then well suited for long duration missions and for manoeuvers that require a large velocity increment. Among the various space-proven technologies, Hall effect thrusters (HETs) offer a high degree of reliability combined with a large thrust-to-power ratio, which makes them attractive for many space missions [2]. Nowadays, 1 kW class HETs are employed for geosynchronous satellite orbit correction and station keeping. In the near future, 5 kW type Hall thrusters will also perform orbit transfer manoeuvers of observation and communication satellites. In addition, high-power Hall thrusters (∼10–100 kW) are ideal candidates for the primary propulsion engine of space probes during journeys towards far-off planets and asteroids.

A Hall thruster is one example of a discharge in crossed electric and magnetic field configuration [3, 4]. Cross-field discharges are actually encountered in numerous areas. Magnetron, anode-layer and end-Hall type ion sources are, for instance, employed for etching of microstructures and for deposition of high-quality thin coatings [5]. On a more fundamental standpoint, a magnetized plasma column is a suitable tool to investigate various sort of instabilities and transport phenomena [6]. The main components of a Hall thruster are given in figure 1. The low-pressure discharge is confined within an annular chamber with dielectric walls. A

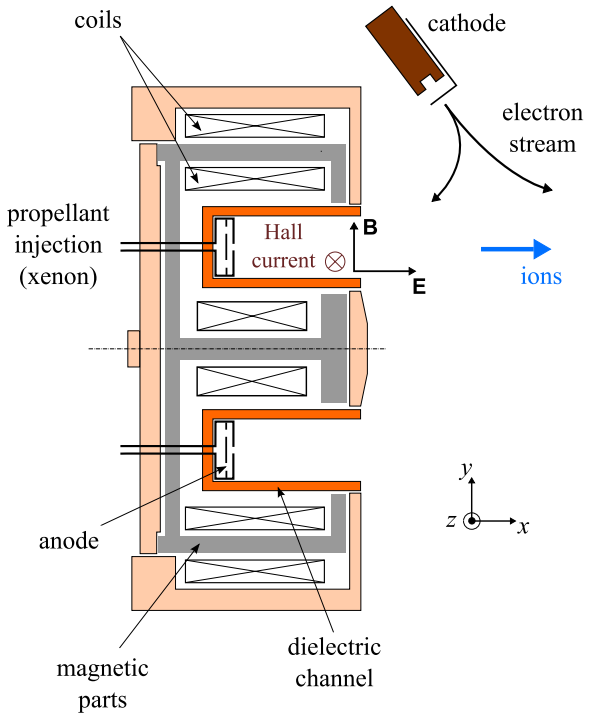

Figure 1. Cross-section view of a HET body in the y–x plane.

set of coils provides a radially directed magnetic field $\boldsymbol{B}$ with a maximum strength at the channel exhaust. The magnetic field is chosen strong enough to trap electrons, but weak enough not to affect ion trajectories. The potential drop is mostly concentrated in the final section of the channel owing to the low electron transverse mobility in this area. The corresponding axial electric field $\boldsymbol{E}$ accelerates ions out of the channel, which generates thrust. The cross-field configuration drives a large electron azimuthal drift: the Hall current. Xenon gas is the usual propellant due to its high atomic mass and relatively low ionization energy.

To a large extent, ion production along with ion acceleration govern thrust level, performance and lifetime. Over the past decade, many experimental works were therefore devoted to the characterization of the Xe^+ ion velocity distribution function by laser spectroscopy in the plasma and the beam of a HET, see, e.g. [7–11]. In contrast, little effort was made to examine the xenon atom transport phenomena. Although indirect, it is an interesting approach to gather complementary information about the ionization region and to better grasp the role of charge-exchange collision events and plasma–wall interactions on Hall discharge behaviour and dynamics. Furthermore, it is also a powerful way of testing and validating various physical models of the $\boldsymbol{E} \times \boldsymbol{B}$ discharge of a Hall thruster. The first study on neutral xenon velocity in a HET was carried out in 1997 by Cedolin *et al* [12] with a low-power device. Probing a metastable state of the xenon atom by means of laser-induced fluorescence (LIF) spectroscopy, they observed a peak in the axial velocity component downstream of the channel exit plane. A few years later, Hargus and Cappelli conducted atom velocity measurements both in the interior and exterior parts of a HET channel for various applied voltages [13, 14]. They confirmed neutrals are accelerated within the thruster whatever the operating conditions. As an explanation, they proposed depletion of the lowest atomic velocity classes due to ionization. In a recent work, Huang and Gallimore examined the axial velocity profiles of resonant and metastable xenon atoms in a high-power Hall thruster [15]. The axial velocity distribution revealed the atom flow accelerates up to the thruster exhaust and it decelerates outside. They also investigated the possible impact of charge-exchange collisions between neutrals and ions.

In this contribution, the lineshape of short-lived and long-lived excited Xe atoms is measured by means of near infrared LIF spectroscopy within the channel and the near-field plume of a 1 kW class HET for various applied voltages. The atom axial velocity component is determined from experimental spectra accounting for the isotopic effect, gas temperature and magnetic field influence. The velocity development along the channel axis is then compared with numerical outcomes of a kinetic/fluid hybrid modelling of the cross-field discharge. The aim of this work is to clarify the contribution of the various phenomena at the origin of the atom flow properties in a Hall thruster.

2. Experimental arrangement

2.1. Optical setup

Laser-induced fluorescence spectroscopy is a non-intrusive diagnostic tool that enables us to determine the velocity of atom and ion species along the laser beam direction by measuring the Doppler shift of absorbed photons. Two electronic transitions are used in this study. The Xe atom in the $6s\,[1/2]^o_2$ resonant level ($1s_2$ level in Paschen notation) is probed by pumping the $6s\,[1/2]^o_2 \rightarrow 6p\,[3/2]_2$ transition at $\lambda = 834.6822$ nm. The resulting fluorescence radiation is captured at 473.41 nm. The Xe atom in the $6s\,[3/2]^o_2$ metastable level ($1s_5$) is probed by exciting the $6s\,[3/2]^o_2 \rightarrow 6p\,[3/2]_2$ transition at $\lambda = 823.1633$ nm. The fluorescence light is then collected at the excitation wavelength.

The LIF optical bench was extensively described elsewhere, see, e.g. [7, 9]. The laser beam used to excite Xe atoms is produced by an amplified tunable single-mode external cavity laser diode operating in the near infrared spectral domain. The wavelength is accurately measured by means of a calibrated wavemeter whose absolute accuracy is 80 MHz (65 m s^{-1}). A confocal scanning Fabry–Pérot interferometer with a 1 GHz free spectral range is used to real-time check the quality of the laser mode and to detect mode hops. The primary laser beam is modulated by a mechanical chopper at a frequency ∼2 kHz before being coupled into a single-mode optical fibre. The fibre allows us to carry the beam into the vacuum chamber of the PIVOINE-2g ground-test facility. The fibre output is located behind the thruster. Collimation optics are used to form a narrow beam that passes through a small hole located at the back of the thruster. The laser beam propagates parallel to the channel centreline in the direction of the ion flow. The laser power density typically reaches 1 mW mm^{-2}, which warrants a weak saturation effect in the case of the 823 nm line. A detection branch made of

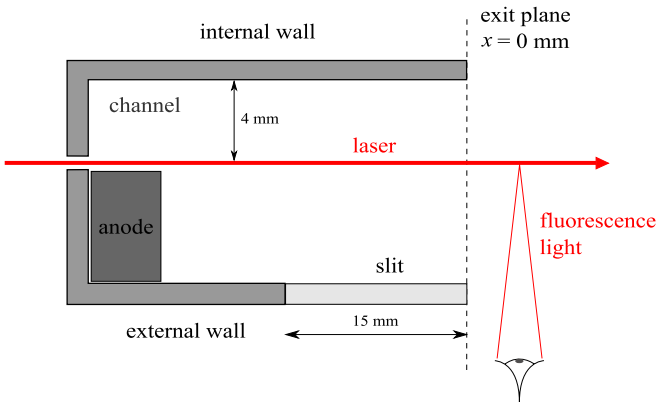

Figure 2. Outline of the laser injection into the channel of the PPS100-ML thruster. Also shown is the detection geometry. The anode-exit plane gap is 25 mm. The channel is 15 mm in width.

a 40 mm focal length lens, which focuses the fluorescence light onto a 200 μm core diameter optical fibre, is mounted onto a travel stage perpendicular to the channel axis. The magnification ratio is 1. A 15 mm slit was made in the channel dielectric outer wall in order to carry out measurements inside the channel. The measurement configuration is shown in figure 2. The channel exit plane is used as a reference; it therefore corresponds to $x = 0$ mm. The fluorescence light is transported with the fibre and subsequently focused onto the entrance slit of a 20 cm focal length monochromator that isolates the observation line from the rest of the spectrum. A photomultiplier tube serves as a light detector. A lock-in amplifier operating at the chopper frequency discriminates the fluorescence light from the intrinsic plasma emission.

2.2. *Hall effect thruster*

The studied Hall thruster, so-called PPS100-ML, is a laboratory model of the Snecma-built PPS100 thruster of which design and dimensions are close to those of the Russian SPT100 thruster. The channel is 25 mm in length. The inner and outer dielectric walls are 70 mm and 100 mm in diameter, respectively. The magnetic field is maximum at the channel exit with $B \sim 150$ G. During the experiments campaign, the thruster was equipped with BN-SiO_2 dielectric channel walls. The xenon mass flow rate injected in the anode Φ_a was kept fixed at 5 mg s^{-1}. In a similar manner, the xenon gas flow rate in the cathode Φ_c stayed at 0.4 mg s^{-1}. The current flowing through coils I_c was changed between 4.5 and 5.5 A. The applied voltage U_d varied from 200 V up to 300 V. The background pressure inside the vacuum chamber was $\sim 2 \times 10^{-3}$ Pa Xe under all conditions.

3. Atomic line profiles

3.1. *Evolution along the channel axis*

The density of Xe atoms in the resonant $1s_2$ state is low due to its short lifetime. As a consequence, the fluorescence signal is lost behind the thruster channel exit plane, which means the atom behaviour can solely be interrogated inside the channel

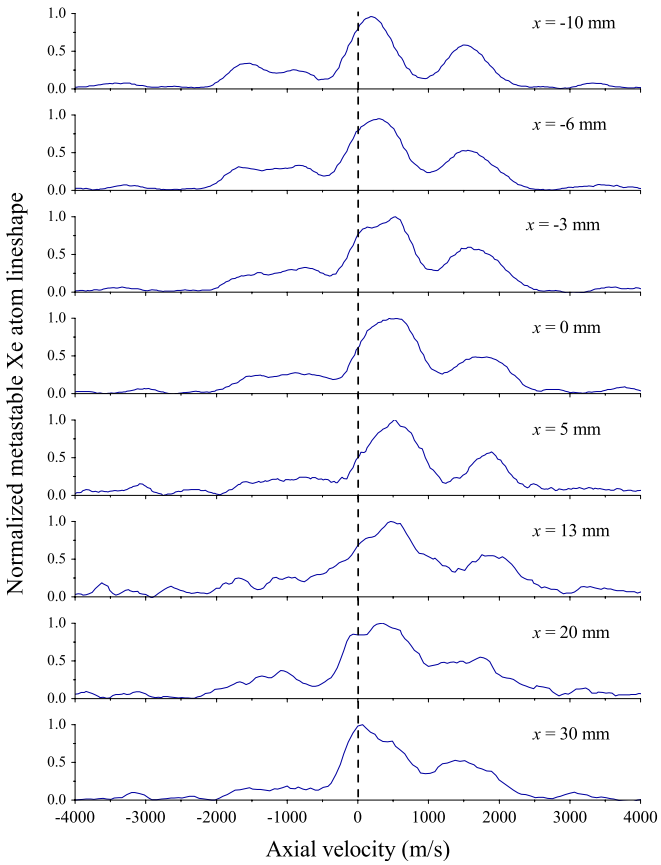

Figure 3. On-axis development of the profile of the 823.2 nm line connected with the Xe $1s_5$ level (250 V and 4.5 A). The position $x = 0$ refers to the channel exit plane.

with the 834.7 nm line. By contrast, a large atomic population is stored in the long-lived $1s_5$ state. The 823.2 nm radiation can then be captured downstream the channel exhaust, which provides information about the atom flow within the thruster plume near-field. In addition, the large lifetime of Xe($1s_5$) atoms under a HET plasma conditions warrants they behave similarly to ground-state Xe atoms [16].

A series of lineshapes that correspond to the $1s_5 \rightarrow 2p_5$ transition at 823.2 nm is displayed in figure 3. Spectra were recorded at several axial positions along a line parallel to the channel axis. The PPS100 Hall thruster was fired at $U_d = 250$ V and $I_c = 4.5$ A. The complicated structure of the line originates from the existence of numerous xenon isotopes. As can be seen in figure 3, the line centre, which corresponds to the atom's most probable velocity, shifts towards large velocity values all the way to the exit plane ($x = 0$). Behind the outlet, the peak shifts in the opposite direction. Note that the Doppler shift always stays positive. Moreover, the line broadens in the course of the flow.

3.2. *Lineshape modelling*

For the two xenon atom excited states, the most probable velocity is given by the Doppler shift of the line centre. In order to extract a larger amount of information from the measured spectra, the profile of the 823.2 nm line was modelled taking into account characteristics of the medium.

The electronic level configuration of Xe atoms is quite complex. The latter exhibits a hyperfine structure which finds its origin in the existence of 7 stable isotopes with abundance above 1%. The hyperfine structure is the result of the combination of two effects: a mass shift due to a slight difference in the electronic configuration of all isotopes and a specific hyperfine structure for odd mass isotope (129 and 131 amu for Xe) due to the existence of a nuclear spin. The selection rule for hyperfine components is connected with the total angular momentum $F = J + I$, where J and I are the electronic angular momentum and the nuclear spin, respectively [17]. For the $6s\,[3/2]^{\circ}_{2} \rightarrow 6p\,[3/2]_2$ transition, the hyperfine constants necessary to calculate energy splittings and the even mass isotope shifts can be found in [18, 19]. The 823.2 nm line is, in fact, composed of 14 hyperfine transitions and 5 isotope-shift transitions. For the latter, intensity is linked to abundance. For each hyperfine component, the intensity is determined from the Clebsch–Gordon factor that depends upon the F, J and I quantum numbers [20].

The influence of the thruster magnetic field upon the electronic levels, the so-called Zeeman effect, must of course be accounted for. A magnetic field induces a splitting of energy levels according to the value of the M magnetic quantum number. The latter also defines the selection rules. As the laser light is unpolarized behind the optical fibre output, both π ($\Delta M = 0$) and σ ($\Delta M = \pm 1$) must be considered. The energy shift is characterized by the value of M_J for even isotopes and M_F for hyperfine components of odd isotopes, the strength of the magnetic field and the Lande factor g_J [17]. The intensity of each Zeeman line is related to the associated Clebsch–Gordon factor. The calculation of the levels shift is performed in the weak field approximation, therefore for hyperfine components the g_F factors are calculated using the quantum numbers F, J and I [20].

After computing the entire line composition, it is necessary to include broadening mechanisms to properly model the lineshape. First, the laser beam profile can be considered as a Dirac delta function in view of the laser bandwidth (<1 MHz). Second, the natural width (5 MHz) is neglected in comparison with the Doppler width that is linked to the gas temperature (∼0.6 GHz at 700 K). The profile of each component is then assumed to be Gaussian. The Doppler width and the Doppler shift are identical for all components. Finally, saturation is taken into account. Broadening of the natural lineshape can here be ignored since the width of the natural lineshape is much below the Gaussian width. Change in the signal amplitude, by contrast, must be considered. The saturation parameter S is the same for all even isotopes as it solely depends on the transition probability. For each hyperfine component of the two odd isotopes, the saturation parameter S has to be divided by the appropriate Clebsch–Gordon factor; so odd isotope contributions are, in fact, less affected by the laser power.

To illustrate modelling outcome, in figure 4 computed line profiles are superimposed onto experimental spectra obtained at $x = -13$ mm and $x = 0$ mm when the PPS100 thruster operates at 250 V discharge voltage with 4.5 A in the coils. The value of the magnetic field amplitude is taken from

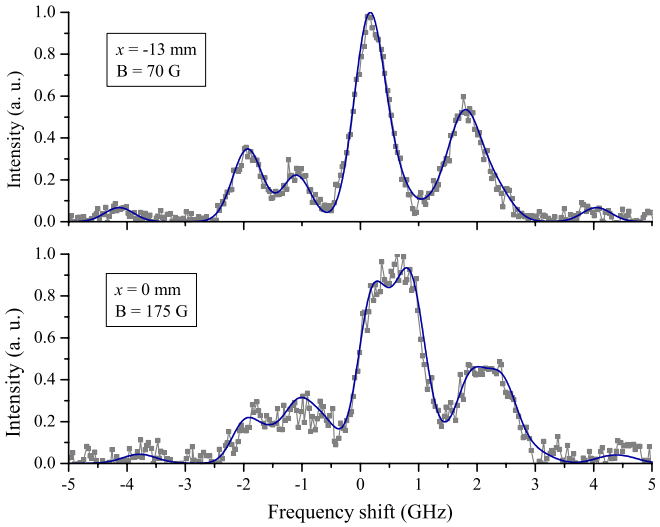

Figure 4. Experimental (square) and computed (line) lineshape for the $1s_5 \rightarrow 2p_5$ transition at 823.2 nm for two locations along the channel axis (250 V and 4.5 A).

measurements. In the two cases, the gas temperature is fixed to 700 K. The gas is here assumed to be in thermal equilibrium with the channel walls of which the temperature was inferred from thermal imaging measurements [21]. The Xe atom mean velocity is then obtained by fitting a calculated spectrum to data points. Note that the saturation coefficient is tuned to match the intensities. As can be seen in figure 4, the agreement between experimental and computed lineshape is satisfactory. This approach allows us to extract fluid quantities with a reasonable accuracy. Inside the channel, the signal-to-noise ratio (SNR) is relatively high. The error bar is $\pm 100\,\mathrm{m\,s^{-1}}$ and ± 150 K for the axial velocity and temperature, respectively. Outside the channel, the SNR diminishes quickly due to the flow expansion. In addition, as we will see in the next section, it is necessary to account for two atom populations to reliably reproduce the measured lineshape, which makes the fitting procedure more complicated. Therefore, error bars grow: $\pm 150\,\mathrm{m\,s^{-1}}$ and ± 200 K.

4. Accelerating and decelerating flow

The evolution of the Xe atom axial velocity component along the channel axis is displayed in figure 5 under various thruster operating conditions. For the resonant $1s_2$ level, the velocity corresponds to the peak of the measured line profile. In the case of the metastable $1s_5$ level the mean velocity arises from a model of the measured lineshape with a gas temperature fixed to 700 K. As can be seen in figure 5, the two probed levels give the same tendency. The atom velocity increases inside the channel from $150\,\mathrm{m\,s^{-1}}$ up to about $600\,\mathrm{m\,s^{-1}}$. Behind the exhaust, the velocity declines gradually towards zero. Curves in figure 5 indicate that varying the discharge voltage and the magnetic field strength has no significant effect upon the velocity profile. The Xe atom axial velocity can be compared with the speed of sound. The latter reaches $272\,\mathrm{m\,s^{-1}}$ at 700 K with a specific heat ratio $\gamma = 5/3$. An apparent subsonic to supersonic transition occurs inside the channel at $x = -5$ mm,

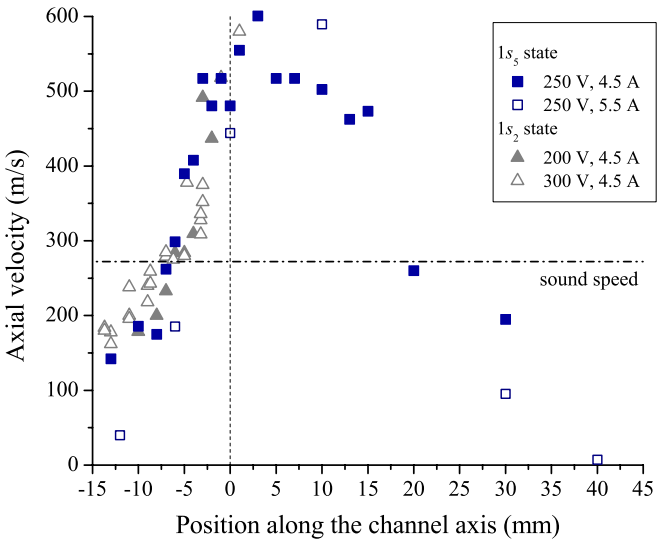

Figure 5. Axial velocity of Xe($1s_5$) and Xe($1s_2$) atoms as a function of the axial position for various Hall thruster operating parameters. Also shown is the speed of sound for 700 K.

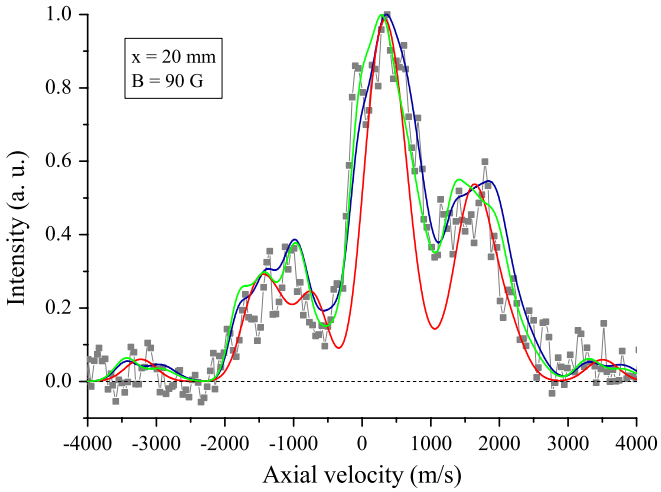

Figure 6. Raw spectrum for the $1s_5 \rightarrow 2p_5$ transition at $x = 20$ mm for 250 V and 4.5 A (square). The red line is the computed lineshape with only a fast atom group at 700 K. Green and blue lines are the sum of a fast component (495 m s^{-1} and 700 K) and a component at rest (300 K) in a population ratio of 70 : 30 and 55 : 45, respectively.

see figure 5. At that location, the mean free path for momentum exchange between Xe atoms is around 1.5 cm. The Knudsen number is then close to unity and the neutral flow is at the limit of the rarefied regime.

Two mechanisms can readily be identified to explain the apparent acceleration of the atomic gas in the interior of the thruster. First, a symmetry break in the velocity space results from the fact that the channel is open on one side. This free-flow effect makes the negative component of the axial velocity weaker and weaker when moving towards the exit plane. As a direct consequence, the peak of the atom velocity distribution function (VDF) shifts towards the positive values. Second, the ionization of slow atoms in the region of large electron density is highly probable owing to their relatively long residence time. Selective ionization is then responsible for the loss of the slow wing of the atom VDF, hence a shift of the mean velocity to the high velocity side [13, 14]. Charge-exchange collision events between Xe atoms and Xe^+ ions lead naturally to the occurrence of a fast atom group. Nevertheless, this process has a little impact upon the atom VDF compared with the two others. As will be shown in the next section, although the proposed physical mechanisms allow us to explain the observed tendency they are, however, not sufficient to explain the measured atomic velocity amplitude.

As can be noticed in figure 5, Xe atoms slow down behind the thruster exhaust. Their velocity reaches zero at $x = 40$ mm. Since no force is acting on atoms, beyond the channel exit plane one expects they form a jet moving with a constant axial speed around 500 m s^{-1} here. The deceleration of the atom flow is actually due to invasion of the jet by atoms that originate both from the hollow cathode and from the background gas. Part of these atoms are locally brought into an excited state by electron impacts. The atom VDF therefore exhibits two components [22]: a fast and hot component that corresponds to atoms from the jet as well as a slow and cold component that comprises atoms from the cathode and the residual gas. This view is supported by the fact that theoretical lineshapes do not conform to experimental spectra when solely considering one group of Xe atoms. In figure 6, the spectrum of the 823.2 nm line acquired at $x = 20$ mm is compared with several calculated spectra. When only one fast atom population is used, the agreement is poor. The agreement is significantly improved with the combination of a fast atom group at 700 K and a standing still group at 300 K. Naturally, the quality of the fit depends upon the population ratio. Two cases are shown in figure 6: a hot-to-cold ratio of 70/30 and 55/45. At $x = 20$ mm, a reasonable fit is obtained when the ratio is 50/50. Note that the uncertainty in the population fraction is large, typically ±30%.

5. Numerical simulations

5.1. Hybrid model

In order to better grasp the physics that drives the flow of atom in the discharge of a HET, experimental data are compared with computer simulations realized with a quasi-neutral transient fluid/kinetic hybrid model developed by the LAPLACE laboratory [23–26]. The latter is based on a quasi-one-dimensional fluid description of the electron transport, while heavy species, i.e. Xe atoms and Xe^+ ions, are treated with a kinetic approach. The computational domain starts at the anode plane and ends at the magnetic field line that intercepts the cathode. The main challenge for the electrons is to properly account for the transport perpendicular to the magnetic field lines. In a HET, cross-field motion is not governed by electron–neutral collisions but by anomalous effects, see [25] and references herein. The cross-field electron mobility profile was determined by means of axial ion velocity profile measurements [26]. To reduce the computation time, the model adopts the macroparticle approach that is commonly used in particle-in-cell model to treat the kinetic description of heavy species. Each macroparticle represents a large number of real particles (ions or atoms). For simplicity sake,

in the rest of the paper, the term ions and atoms refer to macro-ions and macro-atoms, respectively. The ionization profile is calculated assuming a Maxwellian distribution for the electrons, the electron mean energy being obtained solving an energy equation [23]. A given number of ions are created and introduced in the computational domain at fixed positions according to the ionization profile. The equations of motion for ions are solved until they either leave the computational domain or impact on the channel walls. The external force acting on ions is reduced to the electric force due to their large mass. Ions impacting on walls are neutralized and new atoms are reintroduced into the channel.

Neutrals are injected through the anode plane assuming a half-Maxwellian velocity distribution with a temperature of 800 K. A Monte Carlo technique is used to remove neutrals according to the ionization profile. Atoms colliding with channel walls are reflected back assuming diffusive scattering. Ions can naturally recombine at walls to form atoms, which go back with a fraction of the parent ion energy. The velocity of atoms leaving the walls v_a is then given by [28]

$$v_a = \sqrt{\alpha_w v_w^2 + (1-\alpha_w)v^2}, \quad (1)$$

where α_w is an accommodation coefficient. In equation (1), v_w is a random speed sampled from a half-Maxwellian velocity distribution at a temperature of 700 K and 500 K for the channel walls and the thruster body front, respectively. Temperatures were taken from thermal imaging measurements [21]. The term v corresponds to the velocity of the incident particle. When ions collide with the walls, the voltage drop inside the sheath is used to calculate the incident energy [24]. The accommodation coefficient α_w is an adjustable parameter. The background pressure p_{back} is of course considered in the simulations. Atoms are introduced from free space edge of the computational domain with a half-Maxwellian velocity distribution at a temperature of 300 K. Charge-exchange as well as elastic collisions between ions and neutrals are also taken into account [27]. The influence of charge-exchange collision events on the thruster performances is weak in agreement with outcomes of the works by Parra *et al* [29]. Yet, there is an impact on the Xe atom VDF, as we shall be seeing shortly.

5.2. *Computed atom velocity: test cases*

The time-averaged Xe atom VDF was computed along the line of sight for a PPS100 thruster firing at 250 V and 5 mg s^{-1} with 4.5 A in the coils. Several cases were investigated playing with the residual pressure level, the charge-exchange collisions (CEX) and the value of accommodation coefficient α_w. For all cases, the mean axial velocity was determined from the first order moment of the simulated atomic VDF. The on-axis development of the mean velocity was subsequently compared with the acquired data.

First, simulations were carried out neglecting the residual gas pressure ($p_{back} = 0$) with α_w fixed to one, i.e. all Xe atoms are in thermal equilibrium with thruster walls after a collision event, see equation (1). As can be seen in figure 7, computed

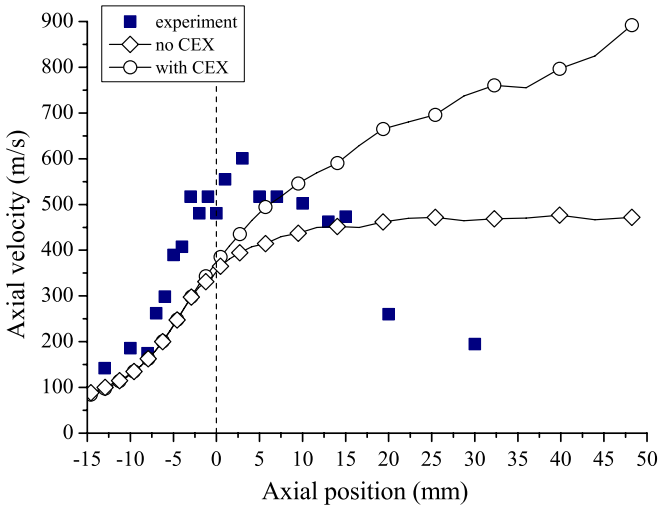

Figure 7. Simulated profile of the Xe atom mean velocity with no backpressure and $\alpha_w = 1$: without (diamond) and with (circle) charge-exchange collisions. Squares correspond to the measured Xe(1s$_5$) atom velocity.

velocity profiles clearly differ from the experimental results. The rise inside the channel is not steep enough. This indicates ionization and free-flow effect are not sufficient to explain the neutral flow acceleration in the interior of the thruster. Moreover, behind the channel exhaust the atom velocity never decreases. The influence of CEX upon the Xe atom flow is clearly seen in figure 7. When CEX are not included into the model, the axial velocity reaches a constant magnitude around 470 m s^{-1}. This value corresponds to the full conversion of thermal energy accumulated inside the channel into kinetic energy. With CEX, the mean velocity increases steadily in the course of the flow. Numerical outcomes show that in spite of a low probability charge-exchange collisions markedly influence the atom VDF.

Second, the background pressure was taken into account in the simulations with $p_{back} = 2$ mPa. Charge-exchange collision were automatically included. The residual pressure has a drastic impact upon the Xe atom velocity as can be seen in figure 8 for e.g. the case $\alpha_w = 1$. In contrast to numerical results plotted in figure 7, this time the axial velocity decreases down to a low value around 100 m s^{-1} behind the channel exit plane. As stated at the end of section 4, deceleration of the atomic flow is due to mixing between hot and fast atoms leaving the channel and slow and cold atoms from the background gas and the cathode. In figure 9, one can observe the computed atom VDF at $x = 10$ mm is indeed made of two distinct components. At $x = 20$ mm, the fraction of fast atoms is 0.65 according to the simulations. This value is in good agreement with the one deduced from modelling of the Xe(1s$_5$) lineshape. Although the shape of the velocity profile is well reproduced with the hybrid model when p_{back} and CEX are incorporated, the calculated velocity magnitude is still in disagreement with the measured one, especially in the channel exhaust vicinity, see figure 8.

In the third case, the value of the accommodation coefficient α_w was changed. Two calculations were made with $\alpha_w = 0.8$ and 0.9, respectively. Fixing the value of the

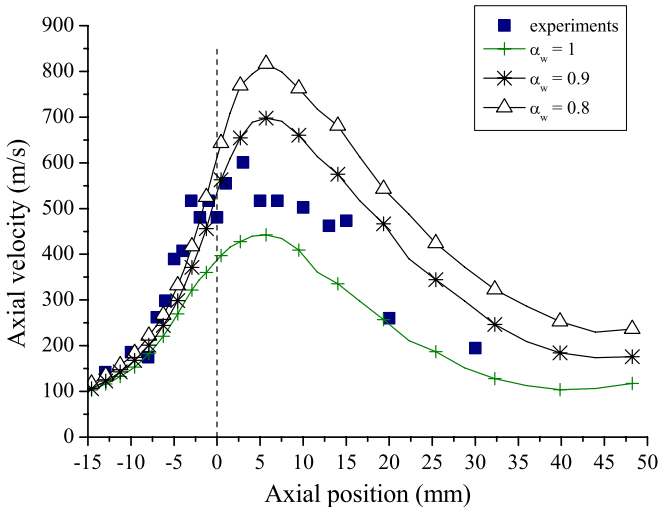

Figure 8. Simulated profile of the Xe atom mean velocity with $p_{back} = 2$ mPa for three values of α_w. CEX are included. Squares correspond to the measured Xe($1s_5$) atom velocity.

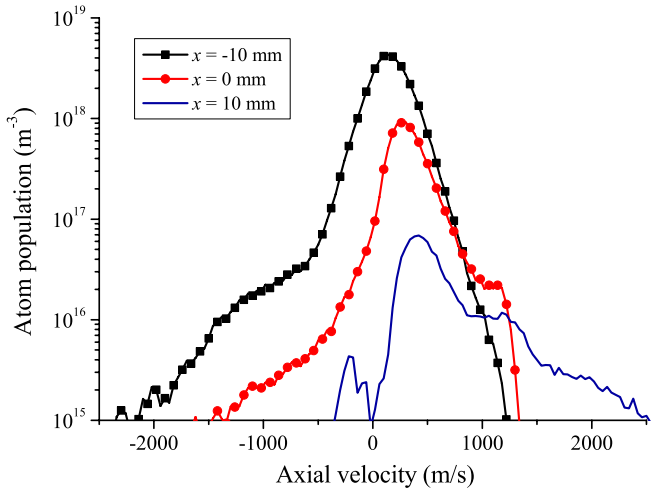

Figure 9. Simulated Xe atom VDF for three axial locations (250 V and 4.5 A). Calculations were performed with the backpressure, charge-exchange collisions and $\alpha_w = 0.9$.

coefficient α_w is rather arbitrary. It is indeed reasonable to think that the accommodation coefficient depends on characteristics of both the incident particle (energy, incidence angle) and the wall materials (composition, roughness). Unfortunately, relevant data are missing for the case of Xe/Xe^+ impacting on BN-SiO_2, which prevents the accurate assessment of the accommodation coefficient. The impact of Xe^+ ions on channel walls of the Hall thruster leads to the creation of a non-negligible fraction of fast atoms when $\alpha_w \neq 1$. The Xe atom VDF plotted in figure 9 shows atoms with an axial velocity above 1000 m s^{-1} inside the channel whereas the thermal speed is 335 m s^{-1} at 700 K. Note that in figure 9 the low atom population with a large negative axial velocity component originates from charge-exchange collisions. The creation of fast atoms naturally occurs in the final section of the channel, a region where the ion energy and the ion flux to the walls are large. In our simulations, the total ion losses on the inner and outer channel walls correspond to 60% of the injected neutral flow, in agreement with the value obtained by Parra *et al* [29]. Curves in figure 8 show the acceleration of the atom flow is reasonably reproduced when $\alpha_w = 0.9$. Simulations therefore indicate the observed rise in the Xe atom velocity results not only from ionization and flow expansion but also from creation of fast atoms at walls due to recombination of ions.

Table 1. Properties of the discharge current I_d as a function of α_w. The quantity σ is the standard deviation and f refers to the main oscillation frequency.

α_w	I_d (A)	σ (A)	f (kHz)
1	4.0	0.5	27.6
0.8	3.6	0.4	28.2
0.5	3.3	0.3	25.5

A last point is worth making. Creation of fast neutrals at walls has a direct impact on the Hall thruster discharge properties. The computed discharge current properties are given in table 1 for three values of α_w. The mean value of the discharge current I_d diminishes with α_w. It is a direct consequence of the drop in plasma density when α_w is turned up. As fast Xe atoms spend a short time inside the channel, their probability of being ionized is low indeed. The main current oscillation frequency stays roughly unchanged. By contrast, the level of oscillation depends on α_w, as shown in table 1. The relationship between I_d and α_w is not yet fully grasped but it surely finds its roots in the prey–predator dynamics that takes place in the cavity of Hall thrusters [30, 31].

6. Conclusion

The flow properties of Xe atoms were investigated in the 1 kW class PPS100-ML HET by means of LIF spectroscopy in the near infrared domain. Fluorescence spectra of the $6s\,[1/2]^o_2$ resonant level and the $6s\,[3/2]^o_2$ metastable level were acquired along the channel axis under several thruster operating conditions. Analysis of the measured lineshapes indicates the atom axial velocity increases inside the channel to a value well above the sound speed before decreasing quickly in the near-field plume. Numerical simulations performed with a hybrid model allow us to explain the shape of the velocity profile. Atomic flow acceleration originates in the combination of three processes, namely the selective ionization of slow atoms, the flow expansion and the creation of fast neutrals on BN-SiO_2 walls owing to recombination of ions. The last process, which was never considered so far, plays a key role in the atom dynamics and discharge properties. Deceleration results from the invasion of the atomic jet by slow and relatively cold atoms from the residual background gas and from the cathode. In addition, it is shown that charge-exchange collisions have a non-negligible impact on the atom velocity in spite of the low background pressure level in ground-test chambers.

Two complementary set of experiments are of interest to confirm the current picture of the atom flow in the discharge of a Hall thruster. The Xe atom velocity profile must be measured with different channel wall dielectric materials, e.g. Al_2O_3, AlN and BN. The goal is here to get deeper insights into the role

of ion recombination. Moreover, the influence of the residual gas on the atom VDF must be clarified. The neutral velocity must of course be measured for various backpressure levels. Another interesting approach consists in injecting a tracer in the tank, such as Kr atoms, and in following its path in the near-field plasma plume and in the channel.

Acknowledgments

The authors wish to thank Dr Nader Sadeghi from the Joseph Fourier University in Grenoble for fruitful exchanges. The authors also want to thank G J M Hagelaar and L C Pitchford from the LAPLACE for helpful discussions. This study was performed in the framework of the joint-research program CNRS/CNES/SNECMA/Universities 3161 entitled '*Propulsion par plasma dans l'espace*'. G Bourgeois benefits from a CIFRE PhD grant (no 286/2009).

References

[1] Turner M J L 2005 *Rocket and Spacecraft Propulsion* (Chichester, UK: Spinger-Praxis Publishing)
[2] Goebel D M and Katz I 2008 *Fundamentals of Electric Propulsion* (Hoboken, NJ: Wiley)
[3] Zhurin V V, Kaufmann H R and Robinson R S 1999 *Plasma Sources Sci. Technol.* **8** R1
[4] Kim V 1998 *J. Propulsion Power* **14** 736
[5] Anders A 2005 *Surf. Coat. Technol.* **200** 1893
[6] Jaeger S, Pierre T and Rebont C 2009 *Phys. Plasmas* **16** 022304
[7] Gawron D, Mazouffre S, Sadeghi N and Héron A 2008 *Plasma Sources Sci. Technol.* **17** 025001
[8] Hargus W A Jr and Charles C S 2008 *J. Propulsion Power* **24** 127
[9] Mazouffre S, Kulaev V and Pérez-Luna J 2009 *Plasma Sources Sci. Technol.* **18** 034022
[10] Mazouffre S, Gawron D and Sadeghi N 2009 *Phys. Plasmas* **16** 043504
[11] Hargus W A Jr and Charles C S 2010 *J. Propulsion Power* **26** 135
[12] Cedolin R J, Hargus W A Jr, Storm P V, Hanson R K and Cappelli M A 1997 *Appl. Phys.* B **65** 459
[13] Hargus W A Jr and Cappelli M A 2001 *Appl. Phys.* B **72** 961
[14] Hargus W A Jr and Cappelli M A 2002 *J. Propulsion Power* **18** 159
[15] Huang W and Gallimore A D 2009 *Proc. 31st Int. Electric Propulsion Conf. (Ann Arbor, MI)* paper 09-87
[16] Small-Warren N E and L-Y Chow Chiu 1975 *Phys. Rev.* A **11** 1777
[17] Saloman E B 2004 *J. Phys. Chem. Ref. Data* **33** 765
[18] Damico G, Pesce G and Sasso A 1999 *Phys. Rev.* A **60** 4409
[19] Suzuki M, Katoh K and Nishimiya N 2002 *Spectrochemica Acta* A **58** 2519
[20] Woodgate G K 1980 *Elementary Atomic Structure* (Oxford: Clarendon)
[21] Mazouffre S, Echegut P and Dudeck M 2007 *Plasma Sources Sci. Technol.* **16** 13
[22] Vankan P, Mazouffre S, Schram D C and Engeln R 2005 *Phys. Plasmas* **12** 102303
[23] Hagelaar G J M, Bareilles J, Garrigues L and Boeuf J P 2002 *J. Appl. Phys.* **91** 5592
[24] Garrigues L, Hagelaar G J M, Boniface C and Boeuf J P 2006 *J. Appl. Phys.* **100** 123301
[25] Adam J C *et al* 2008 *Plasma Phys. Control. Fusion* **50** 124041
[26] Garrigues L, Pérez-Luna J, Lo J, Hagelaar G J M, Boeuf J P and Mazouffre S 2009 *Appl. Phys. Lett.* **95** 141501
[27] Piscitelli D, Phelps A V, de Urquijo J, Basurto E and Pitchford L C 2003 *Phys. Rev.* E **68** 046408
[28] Bruno D, Cacciatore M, Longo S and Rutigliano M 2000 *Chem. Phys. Lett.* **320** 245
[29] Parra F I, Ahedo E, Fife J M and Martinez-Sanchez M 2006 *J. Appl. Phys.* **100** 023304
[30] Boeuf J P and Garrigues L 1998 *J. Appl. Phys.* **84** 3541
[31] Barral S and Ahedo E 2009 *Phys. Rev.* E **79** 046401